High-power widely tunable ps source in the visible light based on four wave mixing in optimized photonic crystal fibers

Jean-Christophe Delagnes, Romain Royon, Jérôme Lhermite, Giorgio Santarelli, Hector Muñoz, Timea Grosz, Dia Darwich, Romain Dauliat, Raphaël Jamier, Philippe Roy, et al.

Research Article | Vol. 26, No. 9 | 30 Apr 2018 | OPTICS EXPRESS 11265
Optics EXPRESS

High-power widely tunable ps source in the visible light based on four wave mixing in optimized photonic crystal fibers

JEAN-CHRISTOPHE DELAGNES,[1,*] ROMAIN ROYON,[1,2] JÉRÔME LHERMITE,[1] GIORGIO SANTARELLI,[3] HECTOR MUÑOZ,[4] TIMEA GROSZ,[5] DIA DARWICH,[6] ROMAIN DAULIAT,[6] RAPHAEL JAMIER,[6] PHILIPPE ROY,[6] AND ERIC CORMIER[1]

[1]*CELIA, Centre Lasers Intenses et Applications, Université de Bordeaux-CNRS-CEA, UMR 5107, F-33405 Talence Cedex, France*
[2]*SATT Aquitaine Science Transfert, Bâtiment A31 – 3ème étage, 351, cours de la Libération, F-33405 Talence Cedex, France*
[3]*LP2N (UMR5298), IOGS-Université de Bordeaux -CNRS, 351, cours de la Libération, F-33405 Talence Cedex, France*
[4]*FYLA, Ronda Guglielmo Marconi 12, 46980 Paterna – Valencia, Spain*
[5]*University of Szeged, Dom ter 9, H-6720 Szeged, Hungary*
[6]*Université de Limoges, CNRS, XLIM, UMR 7252, F-87000 Limoges, France*
**jean-christophe.delagnes@u-bordeaux.fr*

Abstract: We present a detailed study on the generation of widely tunable visible light through four wave mixing in specifically designed micro-structured fibers. The fiber's properties are optimized for an efficient conversion to the visible and near infrared with a combined tunability from 620 to 910 nm of a picosecond Yb-doped tunable source for biomedical applications.

OCIS codes: (060.2280) Fiber design and fabrication; (060.5295) Photonic crystal fibers; (190.4380) Nonlinear optics, four-wave mixing.

References and links

1. T. Gottschall, T. Meyer, M. Baumgartl, C. Jauregui, M. Schmitt, J. Popp, J. Limpert, and A. Tünnermann, "Fiber-based light sources for biomedical applications of coherent anti-Stokes Raman scattering microscopy," Laser Photonics Rev. **9**(5), 435–451 (2015).
2. T. Gottschall, T. Meyer, M. Schmitt, J. Popp, J. Limpert, and A. Tünnermann, "Four-wave-mixing-based optical parametric oscillator delivering energetic, tunable, chirped femtosecond pulses for non-linear biomedical applications," Opt. Express **23**(18), 23968–23977 (2015).
3. E. A. Golovchenko and A. N. Pilipetskii, "Unified analysis of four-photon mixing, modulational instability, and stimulated Raman scattering under various polarization conditions in fibers," J. Opt. Soc. Am. B **11**(1), 92–101 (1994).
4. R. Stolen, "Phase-matched-stimulated four-photon mixing in silica-fiber waveguides," IEEE J. Quantum Electron. **11**(3), 100–103 (1975).
5. W. Wadsworth, N. Joly, J. Knight, T. Birks, F. Biancalana, and P. Russell, "Supercontinuum and four-wave mixing with Q-switched pulses in endlessly single-mode photonic crystal fibres," Opt. Express **12**(2), 299–309 (2004).
6. A. Y. H. Chen, G. K. L. Wong, S. G. Murdoch, R. Leonhardt, J. D. Harvey, J. C. Knight, W. J. Wadsworth, and P. St. J. Russell, "Widely tunable optical parametric generation in a photonic crystal fiber," Opt. Lett. **30**(7), 762–764 (2005).
7. F. M. Mitschke and L. F. Mollenauer, "Discovery of the soliton self-frequency shift," Opt. Lett. **11**(10), 659–661 (1986).
8. J. M. Dudley, L. Provino, N. Grossard, H. Maillotte, R. S. Windeler, B. J. Eggleton, and S. Coen, "Supercontinuum generation in air–silica microstructured fibers with nanosecond and femtosecond pulse pumping," J. Opt. Soc. Am. B **19**(4), 765–771 (2002).
9. C. Jauregui, A. Steinmetz, J. Limpert, and A. Tünnermann, "High-power efficient generation of visible and mid-infrared radiation exploiting four-wave-mixing in optical fibers," Opt. Express **20**(22), 24957–24965 (2012).
10. R. Royon, J. Lhermite, L. Sarger, and E. Cormier, "High power, continuous-wave ytterbium-doped fiber laser tunable from 976 to 1120 nm," Opt. Express **21**(11), 13818–13823 (2013).

#322631 https://doi.org/10.1364/OE.26.011265
Journal © 2018 Received 14 Feb 2018; revised 27 Mar 2018; accepted 31 Mar 2018; published 17 Apr 2018

Optics EXPRESS

11. R. Royon, J. Lhermite, G. Machinet, L. Sarger, and E. Cormier, "Continuously tunable sub-ns ytterbium-doped MOPA system for frequency conversion," in CLEO/Europe and EQEC 2011 Conference Digest 2011, p. CJ_P13.
12. D. Nodop, C. Jauregui, D. Schimpf, J. Limpert, and A. Tünnermann, "Efficient high-power generation of visible and mid-infrared light by degenerate four-wave-mixing in a large-mode-area photonic-crystal fiber," Opt. Lett. **34**(22), 3499–3501 (2009).
13. L. Lavoute, J. C. Knight, P. Dupriez, and W. J. Wadsworth, "High power red and near-IR generation using four wave mixing in all integrated fibre laser systems," Opt. Express **18**(15), 16193–16205 (2010).
14. E. A. Zlobina, S. I. Kablukov, and S. A. Babin, "Phase matching for parametric generation in polarization maintaining photonic crystal fiber pumped by tunable Yb-doped fiber laser," J. Opt. Soc. Am. B **29**(8), 1959–1967 (2012).
15. E. A. Zlobina, S. I. Kablukov, and S. A. Babin, "Tunable CW all-fiber optical parametric oscillator operating below 1 μm," Opt. Express **21**(6), 6777–6782 (2013).
16. J. Yuan, X. Sang, Q. Wu, G. Zhou, C. Yu, K. Wang, B. Yan, Y. Han, G. Farrell, and L. Hou, "Efficient and broadband Stokes wave generation by degenerate four-wave mixing at the mid-infrared wavelength in a silica photonic crystal fiber," Opt. Lett. **38**(24), 5288–5291 (2013).
17. J. R. Peñano, D. F. Gordon, and B. Hafizi, "Generation of mid-IR and visible radiation from four-wave amplification of ultrashort laser pulses in transparent dielectrics," J. Opt. Soc. Am. B **30**(3), 708–716 (2013).
18. G. Agrawal, *Applications of Non-Linear Fiber Optics*, 5th ed. (Academic Press, 2012).
19. M. Delgado-Pinar, Y. Li, D. M. Bird, T. A. Birks, and W. J. Wadsworth, "Third Harmonic Generation in Uniform Fibre Nanotapers via Intermodal Coupling," in Conference on Lasers and Electro-Optics 2010, p. CWL4.
20. C. J. McKinstrie and S. Radic, "Parametric amplifiers driven by two pump waves with dissimilar frequencies," Opt. Lett. **27**(13), 1138–1140 (2002).
21. S. P. Stark, F. Biancalana, A. Podlipensky, and P. St. J. Russell, "Nonlinear wavelength conversion in photonic crystal fibers with three zero-dispersion points," Phys. Rev. A **83**(2), 023808 (2011).
22. M. Droques, B. Barviau, A. Kudlinski, G. Bouwmans, and A. Mussot, "Simple Method for Measuring the Zero-Dispersion Wavelength in Optical Fibers," IEEE Photonics Technol. Lett. **23**(10), 609–611 (2011).
23. www.fiberdesk.com
24. A. Kudlinski, R. Habert, M. Droques, G. Beck, L. Bigot, and A. Mussot, "Temperature Dependence of the Zero Dispersion Wavelength in a Photonic Crystal Fiber," IEEE Photonics Technol. Lett. **24**(6), 431–433 (2012).
25. B. T. Kuhlmey, R. C. McPhedran, and C. Martijn de Sterke, "Modal cutoff in microstructured optical fibers," Opt. Lett. **27**(19), 1684–1686 (2002).
26. N. A. Mortensen, J. R. Folkenberg, M. D. Nielsen, and K. P. Hansen, "Modal cutoff and the V parameter in photonic crystal fibers," Opt. Lett. **28**(20), 1879–1881 (2003).
27. K. Saitoh and M. Koshiba, "Empirical relations for simple design of photonic crystal fibers," Opt. Express **13**(1), 267–274 (2005).
28. F. Kaiser, P. Vergyris, D. Aktas, C. Babin, L. Labonté, and S. Tanzilli, "Quantum enhancement of accuracy and precision in optical interferometry," arXiv:1701.01621 [quant-ph].

1. Introduction

Tunable coherent light sources emitting ultrashort pulses in the visible draw a considerable attention due to the increasing number of emerging applications in the academic, industrial as well as biomedical domains [1, 2]. Since very few efficient solid state laser (SSL) materials emitting in this spectral range exist, coherent visible light is commonly produced through non-linear processes. In particular, intense pulses are obtained by either frequency- (second harmonic generation, sum frequency generation …) or parametric-conversion (optical parametric amplification OPA, four wave mixing FWM) from conventional infrared lasers such as Ti:Sapphire based systems or rare-earth doped lasers (with Nd, Er, Yb, …) as they provide sufficient intensity to drive these non-linear processes.

While propagating in fibers, pulses may experience several competing processes [3]. Self- and cross-phase-modulation, nonlinear elliptical polarization rotation due to optical Kerr effect, spontaneous and stimulated Raman scattering (SRS), degenerated four-wave mixing (d-FWM) [4–6], soliton shift [7], supercontinuum generation [8]…, all are effects leading to spectacular modifications of the pulse spectra with either a wide broadening around the central driving field wavelength or simply a shift of the wavelength towards the visible and/or infrared (IR) domains. Although all based on the material non-linear susceptibilities, the properties of the converted light differ notably. Considering the advantages and drawbacks of each of these processes, d-FWM emerges as the most appropriate effect for the efficient

Optics EXPRESS

conversion of near IR moderately intense laser sources with high average power towards widely tunable short and intense pulses in the visible.

The latter phenomenon now constitutes a viable alternative to laser emission as powerful, stable and compact driving sources can now achieve high nonlinear conversion yield [9]. As mentioned above, RE-doped double clad fibers and, in particular the most widespread high power technology of ytterbium (Yb^{3+}) doped fibers, are in this context ideal sources for all-fiber tunable sources based d-FWM. Indeed, they typically deliver average power P ranging from several tens to a hundreds of watts across the Yb^{3+} emission band. Moreover, they support subpicosecond pulse duration and energies up to hundreds of microjoules with record peak powers in excess of GW. Moreover, beyond the relatively large gain bandwidth, Yb systems have demonstrated their agility in terms of wavelength where lasing was recorded over almost 200 nm of uninterrupted bandwidth e.g., from 976 nm to 1150 nm [10, 11]. Finally, their excellent transverse mode quality is suitable for parametric effects in guiding structures, such as periodically poled waveguides, large mode area (LMA) fibers or microstructured nonlinear photonic crystal fibers (PCF) [12]. Indeed, confinement and guiding both ensure strong second as well as third order nonlinear effects even for cw lasers. Consequently, a significant tunability in the visible [9, 12] can be obtained by the transfer of the broad amplification bandwidth of Yb-fiber lasers in LMA fibers with mode field diameter (MFD) of typically 5 to 15 µm ($0.05 \leq NA \leq 0.3$). Moreover, due to energy conservation, FWM from such Yb sources provides additional longer wavelengths also tunable however ranging in the middle infrared [9, 12–16]. Since the MFD varies weakly with the wavelength (typ. 3 to 10%) the process remains efficient (30% across the entire visible range) with a very good beam quality ($M^2 \leq 1.1 - 1.2$).

Here, we report on the development of an all-fiber picosecond source based on d-FWM tunable between 620 nm and 910 nm at the Watt level for the anti-Stokes wave and from 2874 nm down to 1241 nm for the corresponding Stokes wave. This is, to the best of our knowledge, the widest range achieved so far at this power level taking full advantage of the broad tunability of the infrared pump laser. We first discuss the spectral properties of the d-FWM as a function of the non-linear microstructured fiber dispersion curve. Then, we propose and discuss optimized fiber designs with tailored dispersion specifically engineered to properly map the Yb-doped active fibers spectral tunability onto the visible range. We also detail the elaboration, characterization, and implementation of such microstructured fibers. Finally, we report on the conversion to the visible, by means of d-FWM, of a seed picosecond Yb-doped fiber with high energy (50 - 500 nJ), high repetition rate (5 MHz to 1 GHz), continuously tunable over 1020 nm - 1050 nm. We then conclude and draw perspectives on foreseen applications.

2. Theoretical model of d-FWM

The d-FWM is a four wave process occurring in bulk [17] and fibers [18] as well. In waveguides, the phase matching condition reads:

$$\beta^{(s)}(\omega_s) + \beta^{(i)}(\omega_i) - 2\beta^{(p)}(\omega_p) + \beta_{NL} = 0 \qquad (1)$$

where $\beta^{(m)}(\omega_m) = n_{\text{eff}}(\omega_m)\cdot\omega_m / c$ are the propagation constants of the pump ($m = p$), anti-Stokes (signal $m = s$) and Stokes (idler $m = i$) waves and where $\beta_{NL} = 2\gamma P_p$ is the effective nonlinear propagation constant due to Kerr effect ($\gamma = n_2\omega / c A_{\text{eff}}$) induced by the pump with a peak power P_p [16]. Energy conservation for d-FWM sets $\hbar\omega_s + \hbar\omega_i = 2\hbar\omega_p$. In comparison with second order optical parametric generation and OPA in non-centrosymmetric crystals, d-FWM in fibers and waveguides, interaction occurs over much longer distances leading to significant conversion efficiencies, with however moderate intensities. In the former case, (critical) phasematching, and thus spectral tunability, is solely given by the triplet (ω_p, ω_s, ω_i) pump/signal/idler determined by a configuration of several degrees of freedom such as

Optics EXPRESS

crystal orientation, optical delays and beam angles. At contrast, in fused silica waveguides for instance, the medium is centrosymmetric giving third order effects only and thus requiring four interacting waves. Phase matching in this case is driven by fewer degrees of freedom that are directly accessible to users. The dispersion experienced by the waves depends on the core/clad materials, the guiding architecture, and the shape of the transverse modes involved in the process. Therefore, tunable four-wave processes are observed either (i) naturally providing sufficient pump intensity and proper dispersion one (the FWM process is said degenerated) [12] or (ii) by phase matching colors ω_j on different transverses modes (LP_{qr}) with propagation constants β_{qr} (ω_j) [19] or (iii) by tuning the wavelength two pump lasers [20].

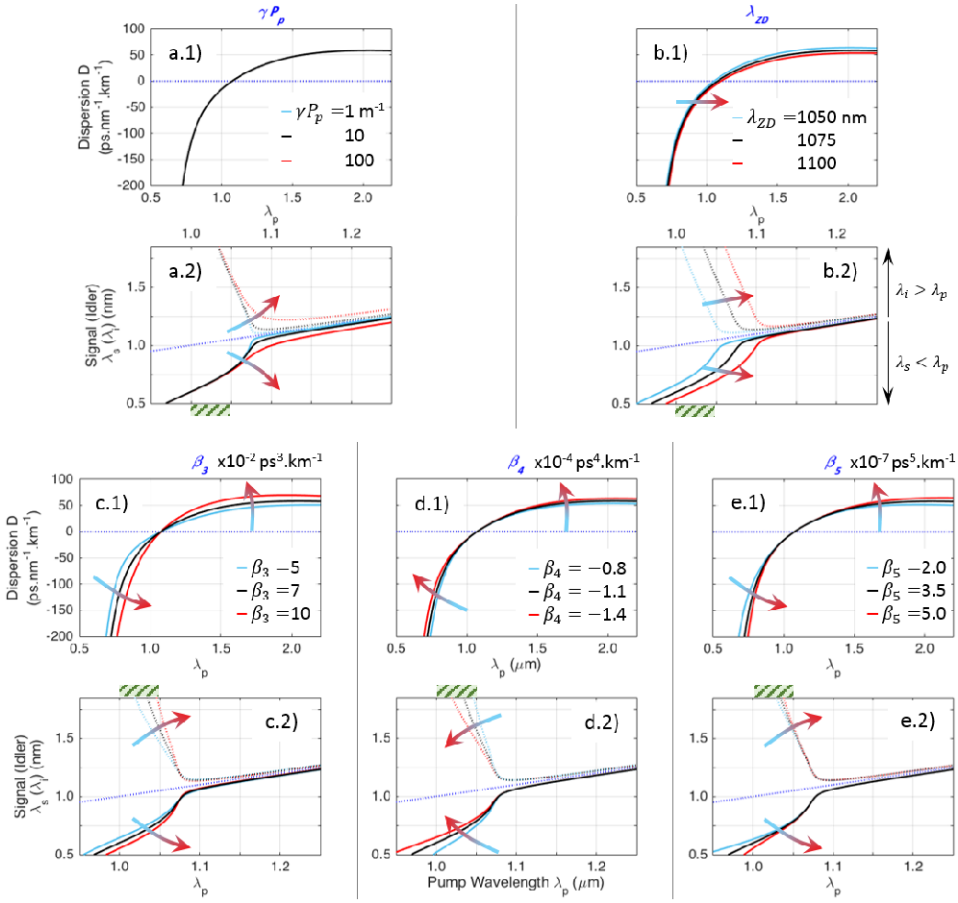

Fig. 1. Influence of the a) nonlinearity γP_p, b) zero-dispersion wavelength λ_{ZD}, and higher order dispersion c) β_3, d) β_4, and e) β_5 on the chromatic dispersion D (a.1 to e.1) and the d-FWM tuning curves $\lambda_{s,i} = f(\lambda_p)$ (a.2 to e.2) for the signal $\lambda_s < \lambda_p$ (solid line) and idler $\lambda_i > \lambda_p$ (dotted line). For each subset a single parameter is varied around the initial set ($\gamma P_p = 10$ m^{-1}, $\lambda_{ZD} = 1075$ nm, $\beta_3 = 7 \times 10^{-2}$ ps^3.km^{-1}, $\beta_4 = -1.1 \times 10^{-4}$ ps^4.km^{-1}, $\beta_5 = 3.5 \times 10^{-7}$ ps^5.km^{-1}) of parameters. The green shaded area marks the actual pump tunability range.

Even with a single pump, large tuning ranges are accessible with dispersion engineered fibers as shown in [21]. The topology of the phase-matching curve depends on the dispersion shape and the number of zero-dispersion points. Photonic crystal fibers (PCF) indeed exhibit numerous advantages for this purpose. First of all, the architecture and the chemical composition (silica SiO_2, germanium GeO_2, high (Boron) and low (Fluorine) index doping) of PCF allow very fine tuning of the dispersion properties. For a given pump tuning range, it is

Optics EXPRESS

thus possible to optimize the signal/idler wavelength excursion. Then, compared to step- or gradient-index fibers, large effective mode area can be obtained in PCF while maintaining single mode operation, and allowing high energy to be converted without damaging the fiber. PCF thus offer the possibility to apply scaling laws [13] in order to simultaneously enable high-power, high-brightness operation, along with broadband tunability across both the visible (signal) and middle-infrared (idler) wavelength range.

In order to engineer a specialty fiber able to cover the visible spectral range through degenerate FWM, we evaluate the d-FWM tuning curves by solving Eq. (1) for the Stokes shift $\Omega = \omega_s - \omega_p = \omega_p - \omega_i$. In order to ease solving, a Taylor expansion up to the fifth order around the zero-dispersion ω_{ZD} is applied to the propagation constants:

$$\beta^{(m)}(\omega_m) \approx \beta_0 + \beta_1 \cdot (\omega_m - \omega_{ZD}) + \tfrac{1}{2}\beta_2 \cdot (\omega_m - \omega_{ZD})^2 + \tfrac{1}{3!}\beta_3 \cdot (\omega_m - \omega_{ZD})^3 + \cdots$$

where $\beta_n = \left(\mathrm{d}^n\beta / \mathrm{d}\omega^n\right)_{\omega_{ZD}}$. The Stokes shift thus reads:

$$\Omega(\omega_p) = \left(-\left(q + \sqrt{q^2 - 4p\beta_{NL}}\right)\Big/ 2p\right)^{1/2} \tag{2}$$

with $p = (\beta_4 + \beta_5 \cdot (\omega_p - \omega_{ZD}))/12$, and $q = \beta_3 \cdot (\omega_p - \omega_{ZD}) + \beta_4 \cdot (\omega_p - \omega_{ZD})^2/2 + \beta_5 \cdot (\omega_p - \omega_{ZD})^3/6$ leading to an improved version of Eq. (2) from [15].

Table 1. Parameters used in the calculation

Parameters	**Values**
Pulse Energy	25 – 300 nJ
Rep. Rate	10 MHz
Avg. Power	0.25 – 3 W
Pulse Duration (Gaussian)	50 ps (FWHM)
Central Wavelength	1020 – 1050 nm
@ 1054 nm: β_3	$+6.9 \times 10^{-2}$ $\mathrm{ps^3 \cdot km^{-1}}$
β_4	-1.11×10^{-4} $\mathrm{ps^4 \cdot km^{-1}}$
β_5	$+0$ $\mathrm{ps^5 \cdot km^{-1}}$
MFD	5 µm
Transparency range	400 – 2200 nm
Nonlinear Index n_2	3.2×10^{-20} $\mathrm{m^2/W}$
$R(t) = (1 - f_R)\delta(t) + f_R h_R(t)$	$f_R = 0.18$
$h_R(t) = H(t)\frac{\tau_1^2 + \tau_2^2}{\tau_1 \tau_2^2}\sin(t/\tau_1)\exp(-t/\tau_2)$	$\tau_1 = 12.2$ fs, $\tau_2 = 32$ fs

From Eq. (2), we can isolate the individual contribution of each terms γP_p, $\lambda_{ZD} = 2\pi c/\omega_{ZD}$, β_3, β_4, and β_5 on the chromatic dispersion D and the phase matching curves. These are reported on Fig. 1 for a large span of pump wavelengths. The actual pump tunability (1020 nm to 1050 nm) is also reported on the graphs (green shaded area Fig. 1(a.2), 1(b.2) and 1(c.2) to 1(e.2)) to estimate the accessible spectral range in the visible at a glance. These graphs serve as a guide for defining the fiber properties. First of all, as depicted in Fig. 1(a.2), the nonlinear dephasing γP_p mainly affects the tuning curve in the vicinity of the ZDW and can thus be neglected in most cases since the pump is far from the ZDW. Then, a change in the ZDW only results in a shift [see Fig. 1(b.2)] along of the blue dotted line $\lambda_s = \lambda_i = \lambda_p$, whose tuning slope $\delta = \mathrm{d}\lambda_s/\mathrm{d}\lambda_p$ remains practically unchanged. In this case, only the signal

Optics EXPRESS

spanning is shifted to the "blue" as the ZDW increases. Similarly, a change in β_3 does not affect the slope [Fig. 1(c.2)], and the signal spanning is shifted to the "blue" as β_3 is increased. Finally, although β_4 and β_5 do not alter the chromatic dispersion D in the same manner [Fig. 1(d.1) and (e.1)], they both affect the slope of the tuning curves [Fig. 1(d.2) and (e.2)] while maintaining a similar behavior close to ZDW. It is noteworthy that – at least in conventional hexagonal structure – β_3 and β_4 exhibit a correlation as shown in [22], preventing from a fully independent adjustment.

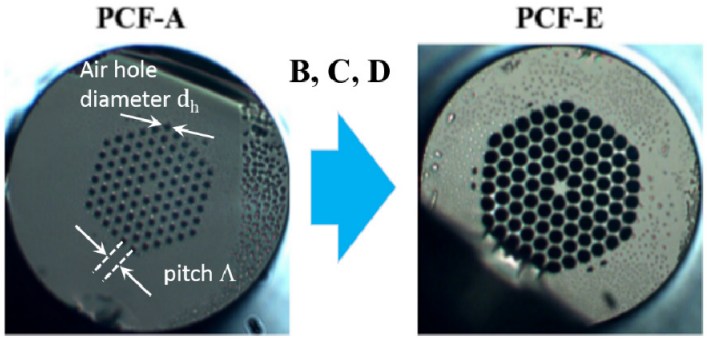

Fig. 2. Microscope images of the cross-section of the A and E PCFs fabricated.

Extensive propagation simulations have been carried out using the commercial software FiberDesk [23] to solve the extended nonlinear Schrödinger equation (NLSE) for the electric field envelope giving access to the complete dynamics (pulse amplitude, gain, spectral build-up, timing, …). Here, we typically solve:

$$\frac{\partial A}{\partial z} = \sum_{n\geq 1} \beta_n \frac{i^n}{n!} \frac{\partial^n}{\partial T^n} A + \cdots \\ \cdots - \int \frac{\alpha(\omega)}{2} \tilde{A}(\omega) e^{-i\omega T} \mathrm{d}\omega + i\gamma\left(1 + i\tau \frac{\partial}{\partial T}\right)\left(A \int R(t') \left|A(T-t')\right|^2 \mathrm{d}t'\right) \quad (3)$$

where $\alpha(\omega)$ is the linear absorption spectrum, $\tau^{-1} = \omega_p$ the "shock" time for self-steepening, and $R(t)$ the normalized function accounting for both the instantaneous electronic and delayed Raman response. In this scalar 1D simulation neither transverse mode structure, nor vectorial effects (polarization) were included.

Table 2. Fibers Characteristics: Geometrical factors, MFA and Nonlinear coefficient

Fiber	Core (µm)	d_h (µm)	Λ (µm)	MFA (µm^2)	γ (W^{-1}.km^{-1})
				Simul.	Simul.
PCF-A	6.5	2.4	4.6	24.3	7.99
PCF-B	5.8	2.3	4.4	22.3	8.71
PCF-C	5.7	2.6	4.3	17.5	11.1
PCF-D	5.3	3.6	4.8	18.7	10.4
PCF-E	4.8	5.1	5.7	18.8	10.3

3. Non-linear fiber design

In order to manufacture non-linear fibers optimized for d-FWM in the visible, we have investigated several hexagonal structures based on the use of air and pure silica as well as others materials composition such as boron (B) or fluorine (F) doped rods. For each architecture, the eigenmodes have been computed with finite element methods giving access to the frequency dependent propagation constant $\beta(\omega)$ and from which the zero dispersion wavelength λ_{ZD} is deduced. The effective nonlinear coefficient γ is extracted from the calculated MFA and the silica core nonlinear index ($n_2 = 3.2 \times 10^{20}$ m^2·W^{-1}). Finally, the

Optics EXPRESS

successive derivatives β_n (up to the 5th order) are numerically obtained from $\beta(\omega)$ and injected in Eq. (1) by developing $\beta^{(m)}(\omega_m)$ ($m = p, s, i$) in the vicinity of $\omega_{ZD} = 2\pi \cdot c/\lambda_{ZD}$.

At this stage, among the different theoretically investigated fiber structures (see Table 2), only the air/silica fibers have been drawn (Fig. 2), characterized and tested. PCFs have been fabricated by the well-known stack-and-draw process. During the drawing, variations have been applied on the gas pressure filling the air-holes of the cladding allowing to obtain several hundreds of meters of different samples characterized by different d_h/Λ ratio. Based on the actual measurement of the fiber profile (Table 2), we simulated the Mode Field Area (MFA) and inferred the nonlinear factor γ. The nonlinear factors are in agreement with those reported in the literature [15].

4. Results and discussion

4.1 Experimental set-up

Our experimental set-up is an all-fiber MOPA configuration (Master Oscillator Power Amplifier) depicted in Fig. 3. The seeder source consists of a home-made Yb-doped fiber laser continuously tunable from 1020 nm to 1050 nm and delivering $\lesssim$ 50 ps pulses at a repetition rate of 10 MHz with a minimal average power of 1 mW over the entire tuning range. Note that the pump spectral range can be extended up to 1080 nm, however with decreasing power as the wavelength reaches the Yb gain curve edge. The seed signal is then successively amplified in two fibered amplification stages to reach a power level of 4 W (which can be further amplified up to 20 W). The first stage is a 2 m long 6/125 µm Yb-doped fiber core-pumped with 500 mW, while the second stage is a 1.8 m long 40/200 µm Yb-doped microstructured fiber clad-pumped with 9 W. While all the results presented here were obtained at 10 MHz, the repetition rate of our source has wide excursion from 5 MHz to 1 GHz not compatible with fiber optical parametric oscillator architectures that operate at rather fixed repetition rates.

The d-FWM visible emission is thus obtained in single pass configuration by focusing the pump in the manufactured microstructured fibers [see Table 2] with a $f = 8$ mm lens (coupling efficiency of 80%). We have observed a degradation of the input facet of the fibers for powers above 3.5 W. It results in a decrease of the coupling efficiency limiting the d-FWM. It, however, can be circumvented with the use of end-caps (not implemented in the present study). Consequently, the maximum average pump power considered in the present study is limited to 3 W. The pump polarization state can be adjusted with a half wave plate but only little dependence has been observed, indicating a slight birefringence of the (non-PM) fibers induced by slight structural inhomogeneities.

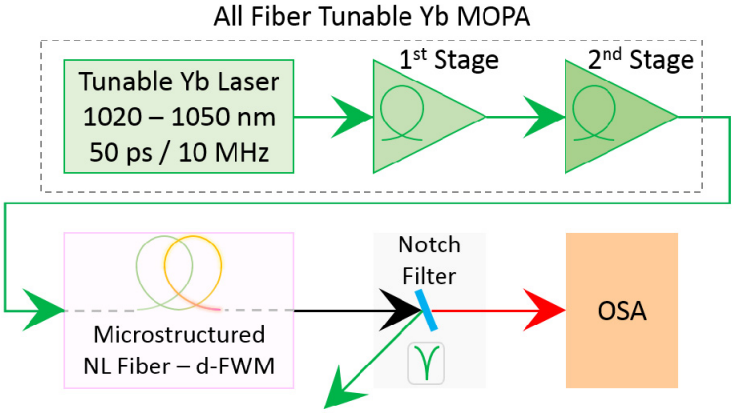

Fig. 3. Schematic of the tunable source.

Optics EXPRESS

Both Raman and d-FWM occur during propagation in the fiber. This has been observed experimentally and confirmed numerically (see Section 4.4). From an initial fiber length of ~1.2-1.5 m, a cut-back is performed down to 0.8 m in order to minimize the onset of Raman scattering. The whole spectrum (signal + pump + idler) is measured from 350 nm to 1750 nm using an Optical Spectrum Analyzer (OSA) Ando AQ6315E. The power is measured after a dichroic mirror separating the signal from the pump and idler.

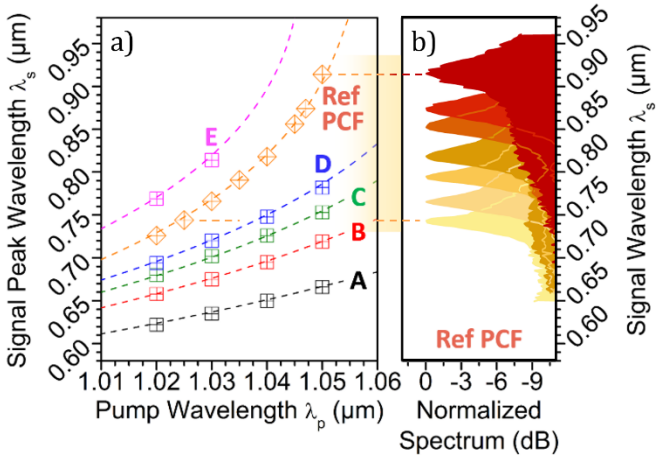

Fig. 4. (a) d-FWM tuning curves (maximum of the signal spectra) on the signal branch (anti-Stokes) for the six fibers tested (PCF-A to -E and Ref PCF, see text for details), and (b) signal spectra for different pump wavelength (obtained with Ref PCF).

4.2 Tuning curves

For all the fibers drawn (PCF-A to -E), we report in Fig. 4(a) the signal central wavelength for pump wavelengths of λ_p = 1020, 1030, 1040 and 1050 nm. Also, for comparison we include the results from a reference air-silica fiber (Ref-PCF) used in the same conditions. The measured signal spectra are reported in Fig. 4(b).

Table 3. Fibers characteristics: dispersion parameters and tuning slopes

Fiber	λ_{ZD} (μm)	λ_{ZD} (μm)	β_3/β_4 (10^2 ps^{-1})	β_3/β_4 (10^2 ps^{-1})	δ @ 1020 nm (nm.nm^{-1})
	WLI	d-FWM	Simul.	d-FWM	d-FWM
PCF-A	1.194	1.137 ± 0.007	−5.83	−6.90	1.47
PCF-B	-	1.101 ± 0.008	−5.95	−6.73	2.03
PCF-C	-	1.095 ± 0.006	−6.18	−6.48	2.43
PCF-D	1.099	1.082 ± 0.003	−6.35	−6.63	2.92
PCF-E	-	1.048	−6.02	-	4.50
Ref-PCF	-	1.054	-	−8.04	4.24

The Ref-PCF, identical to the one studied in [12], serves as a point of comparison in our study. It is a polarization maintaining highly nonlinear fiber (γ = 10 W^{-1}.km^{-1}) with a core diameter of 5 μm (LMA 5-PM produced by NKT Photonics). Similar fibers up to 15 μm core diameter have been tested too. Although larger diameters allow shorter visible wavelength generation, they also require more power to efficiently drive the d-FWM. Moreover, single mode guiding properties of very large mode area is sensitive to temperature [24] and thus not easily compatible with the high average power of the Yb-doped sources considered here.

Optics EXPRESS

In Fig. 4(a), the experimental data (symbols) are fitted (dashed line) using Eq. (2) and adapting the procedure described in [22]. As shown in [22], d-FWM can be indeed thought as a powerful investigation tool for determining the fiber dispersion as its tuning curves depend upon the entire dispersion relationship β (ω). We have reported the values of λ_{ZD} and β_3/β_4 obtained by the fitting procedure in Tab. 3. For comparison, we also reported the chromatic dispersion and the corresponding λ_{ZD} of PCF-A et -D measured using white light interferometry (WLI). Finally, the values of β_3/β_4 obtained from the simulation of the fiber design is also reported. It can be shown that the various techniques applied to recover the fiber parameters are in good agreement. In particular the ratio β_3/β_4 which is highly sensitive to the actual small value of β_4. Moreover, it could further be possible from the ratio β_3/β_4 to extract the individual values of β_3 and β_4 (not discussed here), since they exhibit a correlation in hexagonal PCF structures and can be related with a cubic adjustment [22]. Here we have chosen to focus our investigation on the tuning slope δ obtained experimentally [Table 3] for PCF-A to -E. Depending on the design, the slope can be varied by a factor ~3. Ultimately, we are seeking for the highest slope in order to magnify the tunability of the IR pump laser towards the visible. Unfortunately, the highest slopes, and therefore the broadest tunability range are obtained in the reddest part of the visible spectrum. Therefore, optimization will consist in the best trade-off between bandwidth and central wavelength and certainly depends on the application requirements.

4.3 Conversion efficiency

Figure 5 displays the signal average power as a function of the pump power [Fig. 5(a)] and central wavelength [Fig. 5(b)]. At the full pump power of 3 W, we have recorded an average power in excess of 0.7 W (typ. 1W for most cases) continuously tunable (computer controlled) all across the conversion spectral band of each fiber [see Fig. 4(a)]. The corresponding pulse energy is 70 to 100 nJ.

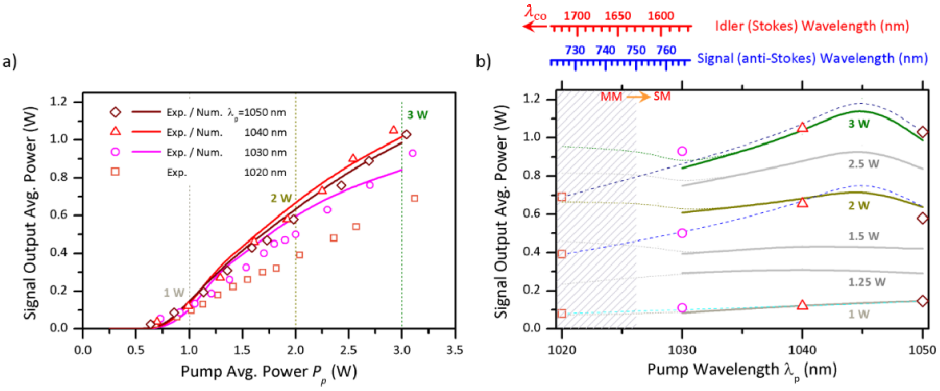

Fig. 5. Experimental (symbols) and simulated (lines) signal output average power at different pump power and wavelength vs. (a) pump average power P_p and (b) pump central wavelength λ_p (□: 1020 nm, ○: 1030 nm, △: 1040 nm, and ◇: 1050 nm for Ref-PCF. The idler (red) and signal (blue) ranges corresponding to the pump wavelength are given atop.

For a better understanding, we have simulated the propagation solving the NLSE (Eq. (3)). Typical parameters used in the simulation are given in Table 1. In particular, we used the dispersion values of $\beta_3 = (6.9 \pm 0.1) \times 10^{-2}$ps^3/km and $\beta_4 = -(1.11 \pm 0.08) \times 10^{-4}$ps^4/km reported in [13]. The power dependence [Fig. 5(a)] gives a remarkably good agreement with the experiments (open symbols) for λ_p = 1040 (△) and 1050 nm (◇). A slight deviation is observed for λ_p = 1030 nm (○), while the simulation fails to quantitatively reproduce the behaviour at λ_p = 1020 nm (□) despite a correct trend. This discrepancy is clearly seen on the

Optics EXPRESS

spectral dependence in Fig. 4(b), where the simulation (solid line) and experiment (open symbols) are in good agreement, except for λ_p < 1030 nm (shaded area) where the experimental trend (dashed line) clearly deviates from the simulation (dotted line) for the highest powers considered here. This discrepancy may find its origin in the (transverse) modal behaviour of the fibers that are multimode [25,26] tends to become more and more multimode (V-number increases [27]) as both the pump and the signal go deeper into the short-wavelength range. Indeed, in the d-FWM process, higher-order transverse modes do not couple efficiently, and the signal gain is consequently decreased.

4.4 Spectrum build-up and optimal fiber length

As depicted in Fig. 4(b), one can see a significant spectral broadening while both the pump and the generated signal approach the ZDW. Moreover, as mentioned above, the onset of Raman scattering has been observed experimentally and a cut-back procedure was required to suppress the process. In order to gather a better understanding related to the two phenomena, we performed simulations using the parameters from PCF-E. The spectral evolution of the three waves (signal, pump and idler) as a function of the propagation distance is reported in Fig. 6.

It is noteworthy that around z = 0.6 m, a sudden broadening occurs for both the Stokes (idler) and anti-Stokes (signal) sidebands. Such a distance barely corresponds to the actual cut-back length we have determined experimentally (z = 0.8 m). Beyond this distance, the conversion efficiency levels off, while Raman contribution progresses (not visible on Fig. 6 on such a scale). We also note the good agreement in the asymmetric broadening of the experimental [Fig. 4(b)] and numerical [Fig. 6] anti-Stokes (signal) spectra.

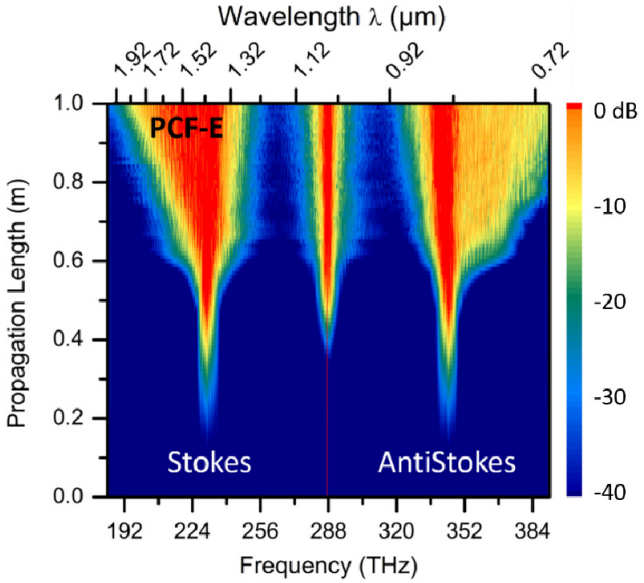

Fig. 6. Simulation of the d-FWM spectrum build-up along the propagation distance z in the PCF-E.

5. Conclusion and perspectives

We have investigated four wave mixing processes in non-linear photonic crystal fibers pumped by a widely tunable seed fiber laser. Beyond the fundamental aspect of FWM, we present a detailed study of specifically designed air-silica fibers to optimally map the large tuning range of the Yb-doped fiber pump laser onto the visible where such a source may find important applications. We demonstrate a tunability of the anti-Stokes wave ranging from 620

Optics EXPRESS

nm to 910 nm with home-made air-silica PCFs and output powers up to 1 W, i.e. energies up to 100 nJ (with 30% anti-Stokes to pump single-pass efficiency). FWM is highly sensitive to the actual fiber parameters and therefore, their values need accuracy. The numerical prediction of the dispersion parameters, although imperfect, is in good agreement with the parameters extracted from the d-FWM phase-matching curves, while the gain and bandwidth are in excellent quantitative agreement with the experiments.

The present study has shown that optimization of the tuning range requires an accurate and absolute knowledge of the dispersion curves, especially for the most extreme Stokes shift when the targeted signal and consequently the idler respectively lie in the "blue" and middle infrared ranges far from λ_{ZD} and central pump wavelength λ_p. As mentioned earlier, a comparison between white light interferometry measurement, d-FWM dispersion measurement and as well as simulations revealed discrepancies. In fact, WLI inherently provides insufficient precision on the ZDW and dispersion coefficients. At contrast, d-FWM allows determining higher dispersion terms with good accuracy. We are quite confident that quantum white-light interferometry (QWLI) [28] will offer a viable alternative for in-line "screening" of short fiber samples as the accuracy is only limited by quantum noise. This would allow testing different layout with high/low index material boron- or fluorine-doped, or core (co-)doping with germanium GeO_2 to adjust the dispersion, confinement (MFA), transparency range and nonlinearity.

Funding

Laserlab-Europe (EC Horizon 2020) (654148), Idex-Laphia (ANR)(ANR-10-IDEX-03-02), Tempus Public Foundation (MÁEÖ2016_3, 74702).

Acknowledgments

We would like to thank L. Merzeau for the optomechanics. JCD would like to thank L. Labonté, S. Tanzilli, C. Valentin, V. Blanchet, S. Petit, F. Burgy for fruitful discussions and/or critical reading.